ELSEVIER

Journal of Structural Geology 36 (2004) 401–418

JOURNAL OF STRUCTURAL GEOLOGY

www.elsevier.com/locate/jsg

Analogue modelling of reverse fault reactivation in strike–slip and transpressive regimes: application to the Giudicarie fault system, Italian Eastern Alps

G. Viola[a,*], F. Odonne[b], N.S. Mancktelow[c]

[a]*Department of Geological Sciences, University of Cape Town, 7700 Rondebosch, South Africa*
[b]*Université Paul Sabatier, Pétrophysique et Tectonique, U.M.R. 5563 C.N.R.S., 38 rue des Trente-six-Ponts, 31400 Toulouse, France*
[c]*Geologisches Institut, ETH, Sonneggstrasse 5, 8092 Zürich, Switzerland*

Received 1 November 2002; received in revised form 1 July 2003; accepted 1 August 2003

Abstract

Sandbox analogue models were used to study the reactivation of a reverse fault in strike–slip and transpressive regimes, for comparison with the evolution of the Giudicarie fault system in the Central Eastern Alps. The Giudicarie system is interpreted as resulting from Late Miocene sinistral transpressive reactivation of an older, Late Oligocene reverse fault. The 'old' reverse fault was reproduced as a pre-cut dilatant surface obtained by pulling a stiff metal wire through the model sand layer. The position of the pre-existing fault with respect to the base plate fault accommodating the strike–slip and transpressive faulting phase controlled the extent and geometry of reactivation. The clearest reactivation in a pure strike–slip regime was achieved in experiments where the basal strike–slip fault was immediately below the pre-existing fault plane. This strong reactivation involved lateral extrusion and lateral stepping of secondary faults from the basal fault to the pre-existing reverse fault. In the case of transpression, the most spectacular reactivation was achieved for a convergence angle of 10°. Strongly asymmetric structures developed on either side of the pre-cut dilatant zone. The analogue experiments reproduced very closely the structural features of the Giudicarie fault system, supporting a model involving a twofold tectonic evolution for the Giudicarie fault system, with later reactivation in sinistral transpression of an older reverse fault.

Keywords: Sandbox experiments; Fault reactivation; Giudicarie Fault System

1. Introduction and aim of the study

Strain on the scale of the lithosphere is often localized into relatively narrow fault and shear zones that produce patterns of deformation involving complex fault geometries and kinematics. These faults form zones of mechanical weakness that influence the architecture, kinematic pattern and distribution of crustal-scale deformation in both continental and oceanic regions. As long as a pre-existing fault remains mechanically weaker than its surroundings, strain is preferentially concentrated in the fault zone. This occurs, irrespective of whether the deformation is continuous or interrupted by periods of little activity, because pre-existing faults are surfaces along which the cohesive strength and the friction coefficient are lower than those of intact rocks (Anderson, 1951). The behaviour of faulted rock is determined by its geometric, kinematic, rheological and historical (inherited) characteristics. Whereas fault kinematics obviously reflect the regional and local stress fields and, more generally, the geodynamic setting, fault geometry is strongly affected by the existence of zones of rheological and mechanical weakness (pre-existing faults) at the time of deformation. Therefore, older inherited structural features have long been recognized as a key factor in controlling strain distribution and localization and much attention has recently been paid to the phenomenon of fault reactivation (e.g. Holdsworth et al., 2001 and references therein). Numerous field studies have provided insights into fault reactivation processes in different tectonic settings and recent developments in techniques such as microfabric analysis, paleomagnetism and high resolution geochronology have helped to recognize multiple deformation phases preserved in the same fault-related rocks. Unfortunately,

* Corresponding author. Tel.: +27-21-6502928; Fax: +27-21-6503783.
E-mail address: gviola@geology.uct.ac.za (G. Viola).

0191-8141/$ - see front matter © 2003 Elsevier Ltd. All rights reserved.
doi:10.1016/j.jsg.2003.08.014

only the final sum of all these deformation stages is available for field study and there is no opportunity to consider the starting point and/or intermediate steps. Moreover, the situation is not improved by the fact that, even for the final geometry, important evidence has been removed by erosion or is still buried. In attempting to decipher this progressive deformation history, the use of analogue models, coupled with a theoretical analysis of the dynamics of tectonic processes, is extremely useful. With the aid of properly scaled models, an experimenter may at least distinguish physically possible theories from impossible ones. The results derived from these models may be studied and analyzed in great detail, allowing the deformation history to be deciphered to an extent not otherwise possible.

Following this approach, we present the results of a series of sandbox analogue experiments performed to test the mechanical and geometrical validity of a large-scale tectonic model proposed by Viola et al. (2001) for the Giudicarie fault system in the Italian Eastern Alps, which forms a prominent component of the orogen-scale Periadriatic fault system. The field and geochronological data presented by Viola et al. (2001) point to a twofold evolution of the Giudicarie fault system, where a major reverse fault was reactivated in a strike–slip/transpressional mode during a later deformation phase. The results of this study stress the importance of fault reactivation processes in modelling tectonic features, even at the orogen scale.

2. The Giudicarie fault system

The Giudicarie fault, located in the Italian Eastern Alps, is a primary segment of the Periadriatic fault system (Fig. 1). The Periadriatic fault system is the most striking structural feature in the whole Alpine chain, separating the Western, Central and Eastern Alps (to the north) from the Southern Alps over a distance of more than 700 km (Fig. 1, e.g., Bigi et al., 1990). The NNE–SSW-trending Giudicarie fault system consists of several faults, with different kinematics, deformation style, and also different periods of activity (Viola et al., 2001 and references therein; Fig. 2). It coincides with a significant modification in the strike direction of the Periadriatic fault system, which otherwise trends generally E–W in the region. This structural peculiarity has recently been a matter of lively debate. Indeed, establishment of whether the break in strike formed by the Giudicarie fault system is an inherited structural feature (pre-Oligocene) or a late, collision-derived structure is crucial for estimating the maximum possible amount of accumulated dextral shearing along the central Periadriatic fault (see Viola et al. (2001) for a thorough analysis). This, in turn, imposes different constraints on the proposed orogen-scale tectonic models. Two schools of thought are current. Some authors propose that the Periadriatic fault, prior to the post-collisional shortening, was a straight E–W striking fault, which was then offset by the indenting Adria promontory (e.g. Schönborn, 1992; Laubscher, 1996; Schmid et al., 1996; Frisch et al., 1998; Schmid and Kissling, 2000). This model requires that the Giudicarie fault is a late structure in the Alpine history, which has sinistrally offset the Periadriatic fault by more than 70 km and excludes major fault reactivation processes.

On the other hand, Viola et al. (2001) present evidence in support of a second model in which, although there has been some sinistral strike–slip displacement accommodated by the Giudicarie fault, the amount of displacement is not simply equivalent to the apparent offset in the approximately E–W segments of the Periadriatic fault (e.g. Castellarin and Vai, 1982; Prosser, 1990, 1998, 2000; Müller, 1998; Müller et al., 2001; Viola et al., 2001). In this model, the Giudicarie fault system has nucleated on a primary, inherited geometrical feature of the original passive margin, which was then partially modified during post-collisional shortening.

The main implication of this reconstruction is that the Giudicarie fault has belonged to the Periadriatic fault system since at least the Oligocene and, as such, has gone through several phases of deformation reflecting a progressive reorientation of the regional stress field. In the Oligocene, during the so-called Insubric phase (e.g. Prosser, 1998), dextral shearing along the Tonale and Pustertal faults was accommodated via thrusting/reverse faulting along the Giudicarie fault, which formed a major restraining bend in the otherwise straight Periadriatic fault. In the Late Miocene, as a consequence of the still ongoing convergence and N–S shortening, the Oligocene thrust-related structures were partially reactivated in a sinistral transpressive regime along (1) the brittle–ductile Passeier fault, (2) along part of the Giudicarie fault sensu stricto itself, and (3) along a series of minor splay faults in the Southern Alps (Fig. 2; Viola et al., 2001). This resulted in the development of strongly asymmetric structures and formed a complex system of splay strike–slip and thrust faults in the Southern Alps (Fig. 2). The maximum sinistral strike–slip displacement during this deformation phase has been evaluated, using a pre-existing structural marker, as between 13 and 15 km (Spiess et al., 2001; Viola et al., 2001).

In order to verify the validity of this tectonic reconstruction, the process of tectonic reactivation of a pre-existing reverse fault (the Oligocene reverse fault in the Giudicarie case) in a strike–slip and transpressional regime (the late Miocene faulting) has been investigated using a series of simple sandbox experiments.

3. Previous models on reverse fault reactivation

Many examples of fault reactivation have been described for various tectonic regimes (e.g. Harding, 1985; Betz et al., 1987; Koopman et al., 1987; McClay, 1989; Richard and

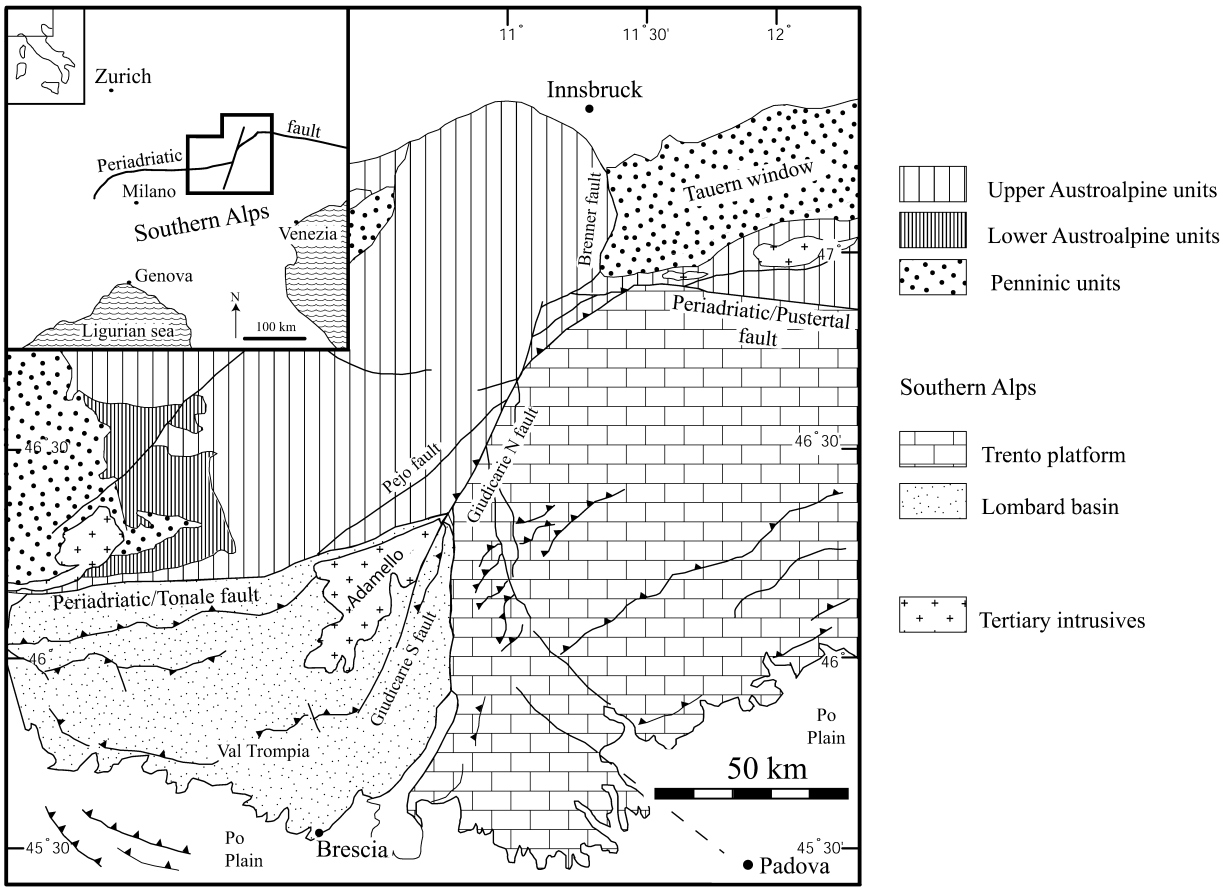

Fig. 1. Simplified geological map of the central Periadriatic fault system in the Giudicarie area (from Viola et al., 2001).

Krantz, 1991; Schreurs and Colletta, 1998), but the dynamic and kinematic processes associated with structural reactivation are still not fully established. Most previous experimental studies simulating fault reactivation in strike–slip regimes considered movement along a single basement strike–slip fault associated with a transverse displacement (convergence) of the longitudinal sidewalls of the model, thus combining wrenching with a shortening component perpendicular to the shear zone (e.g. Richard and Cobbold, 1990). Richard and Cobbold (1990) described a zone of high deformation above the base plate fault and report typical positive flower structures, in which conjugate reverse faults converged towards the base of the model, accommodating vertical extrusion of a wedge with a somewhat rounded surface bulge. In the case of pure sand experiments, the base plate fault exerted a strong control on the spatial location and on the strike of faults. Other studies have instead tried to simulate more distributed deformation by introducing either a rubber sheet (Naylor et al., 1986) or viscous material (Richard and Krantz, 1991; Richard et al., 1995) at the base of the sand layer, immediately above the basement fault. Schreurs and Colletta (1998) imposed an oblique shear component at the base of the model over its entire width in order to simulate oblique deformation of a model driven by distributed basal flow. Oblique shortening (transpression) was obtained by combining a basal, distributed strike–slip shear component with transverse shortening. Richard and Krantz (1991) also performed experiments on fault reactivation in strike–slip mode, using either pure sand models or models including a Newtonian ductile layer of different thicknesses at the base. Each of their models was deformed in two steps: a pure dip–slip stage was followed by a reactivation in pure strike–slip mode. In surface view, minor reactivation was observed in that the deformation imposed during the strike–slip phase was mainly localized along pre-existing dip–slip structures. However, in serial cross-sections, they observed that faults were reactivated at depth. This observation convinced the authors that reactivation of faults in strike–slip mode can occur at depth, without being visible at the surface.

In our new experiments, an attempt was made to improve understanding of the reactivation of a pre-existing reverse fault in pure strike–slip mode and in a transpression regime. The strike–slip models differed from those in the literature in that the importance of the spatial position of the ‘old’ structure with respect to the base plate fault was investigated. In general, it should be noted that reactivation in a transpressional regime is a relatively unknown issue, and these experiments are some of the first to specifically address this problem.

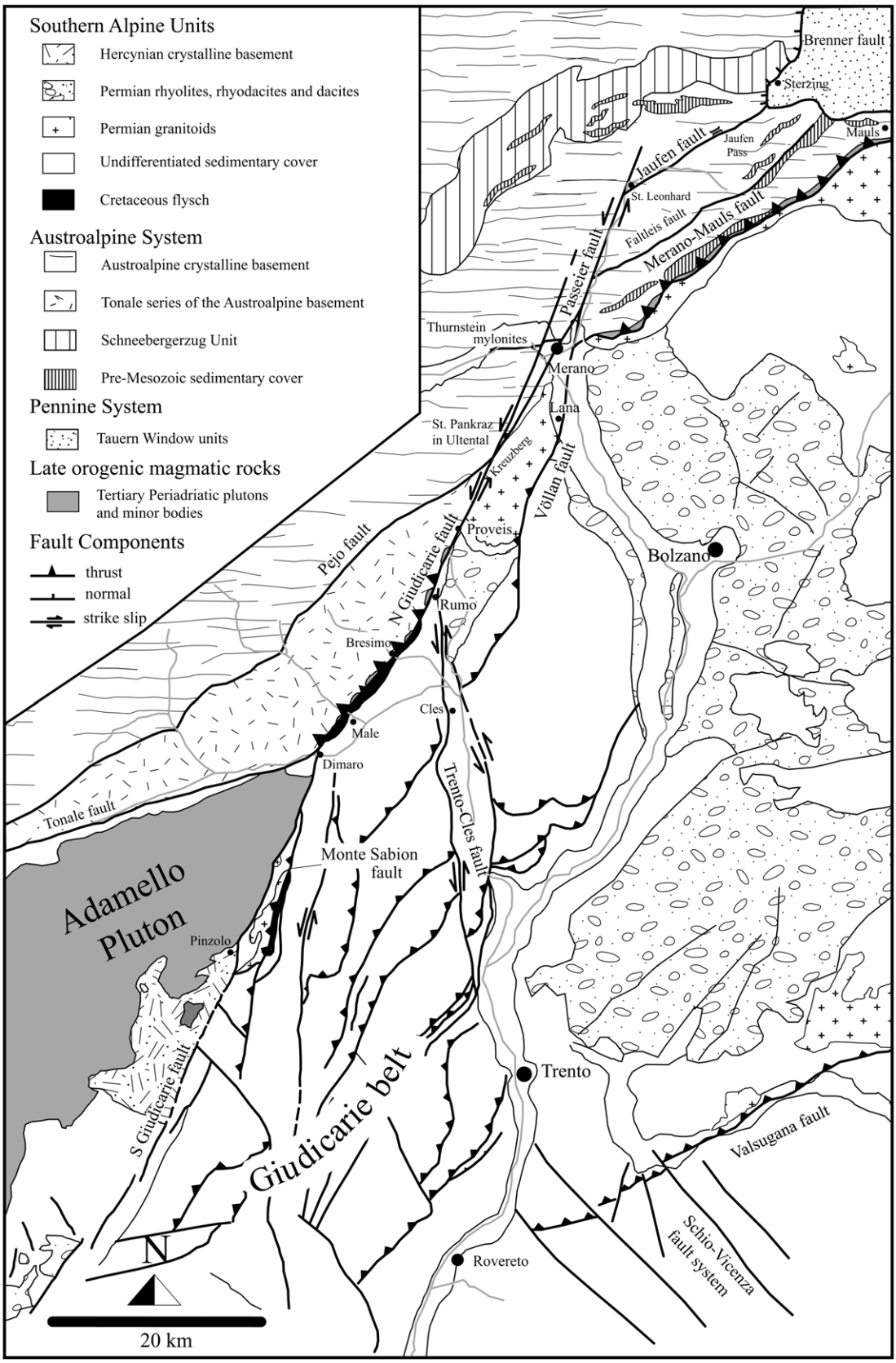

Fig. 2. Detailed tectonic map of the Giudicarie region showing the geometrical arrangement and the kinematics of the main components of the Giudicarie fault system (from Viola et al., 2001).

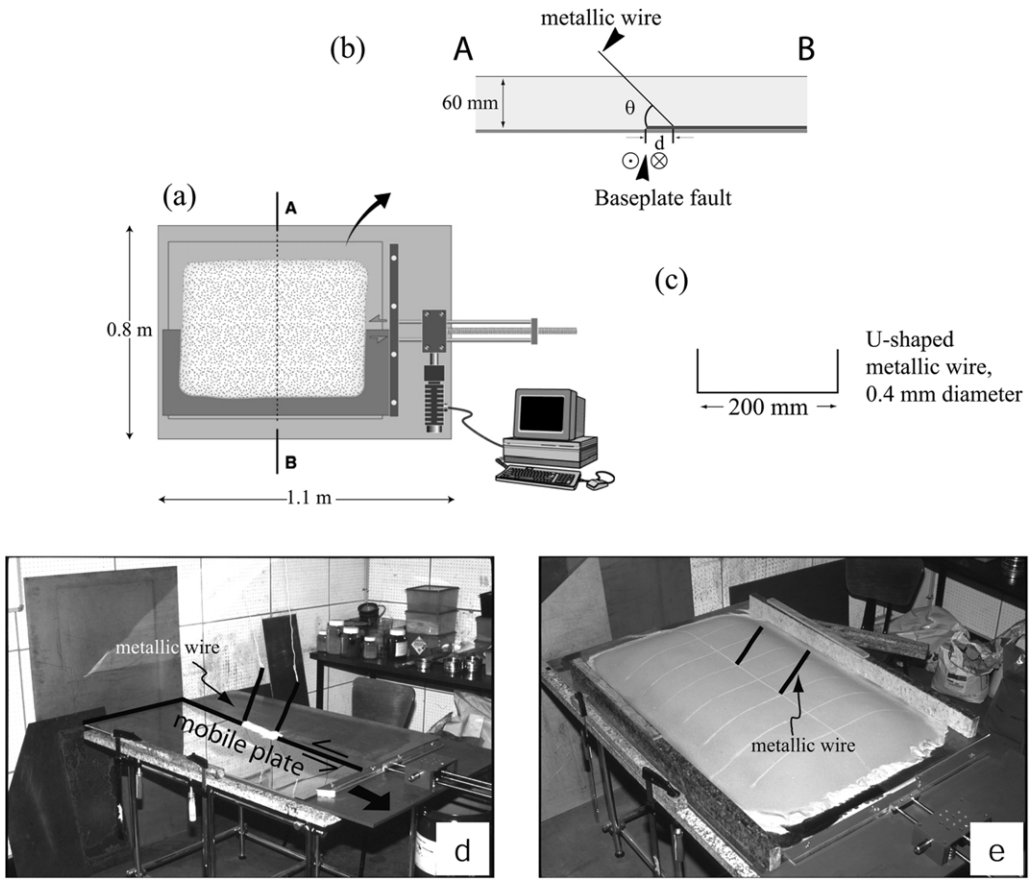

Fig. 3. Experimental apparatus. (a) Plan view of the apparatus showing the metallic plates, the sand layer, the stepper motor and the computer controlling the motor. (b) Section of the sand layer defining the parameters d and θ and showing the sense of relative displacement between the two halves of the experimental apparatus. (c) Shape and dimensions of the metallic wire used to create the dilation zone. (d) and (e) Photographs of the deformation apparatus before ((d), note the shape of the plate used to reproduce transpression) and after (e) sieving the sand. Note the position of the metallic wire.

4. Experimental set-up

The experimental apparatus used in this study consisted of a large table (1.1 m × 0.8 m) on top of which lay a thin metallic plate (Fig. 3). In the case of pure strike–slip deformation, the plate had a rectangular shape and covered only one half of the table. The short side of the plate was fixed by a metal bar to a computer-driven stepper motor that pulled it parallel to the long edge of the table (Fig. 3a). The pre-existing fault was modelled as an artificial dilation zone in the sand cake. To create this zone, a stiff metallic 0.4-mm-thick wire was built into the sand model in the central part of the table and then pulled through the sand at an angle θ to the horizontal of 40–68°, depending on the model (Fig. 3). Unfortunately, it was very difficult to pull the metallic wire manually through the sand model at an exact pre-defined angle from the horizontal. As a result, there is a relatively large variability in the pre-existing fault dip angles. The thickness of sand was ~60 mm throughout the model and the sand layer was laterally unconfined. Sand was manually sifted onto the table and, by adding small amounts of stained sand at regular intervals, a series of coloured marker horizons was obtained. A 100-mm-spaced grid was drawn on the top surface as a reference for evaluating displacements and fault motions. Photographs of the free surface were taken at regular displacement intervals (the brittle deformation is virtually time independent), thus documenting the surface deformation. At the end of each experiment, the model was impregnated with water to give cohesion and cut into vertical slices, perpendicular to the base plate fault. Most sections showed fault traces with finite offsets of the colour banding. Three experiments (GI A, GI B and GI C) were performed in pure strike–slip regime, with the wire placed at decreasing distances from the plate boundary (Table 1), in order to test the influence of the position of the pre-existing reverse fault on the degree of reactivation.

Four other experiments modelled a transpressive deformation regime (Table 1). The oblique shortening component was achieved by using a non-rectangular plate (Fig. 3d). Its long side formed an angle of 85° (experiment GI E) or 80° (experiment GI D and GI K) to the short side, so that an oblique compressive component was transmitted to the sand layer by simple constant velocity displacement of the mobile part of the assembly. In these three experiments, the metal wire was aligned along the plate boundary (Fig. 3d).

Table 1
List of the experiments described in this study and of their geometrical parameters. For the physical meaning of the symbols refer to Fig. 3

Experiment	Deformation type	d (mm)	θ (°)	Convergence angle (°)	Metal wire	Position of metal wire
GI A	Strike–slip	60	50	0	Yes	Parallel to base fault, 60 mm away
GI B	Strike–slip	40	52	0	Yes	Parallel to base fault, 40 mm away
GI C	Strike–slip	0	60	0	Yes	On the base fault
GI G	Transpression	0	–	10	No	–
GI D	Transpression	0	68	10	Yes	On the base fault
GI K	Transpression	0	40	10	Yes	On the base fault
GI E	Transpression	0	45	5	Yes	On the base fault

In experiment GI D the pre-existing fault had a 68° dip angle, whereas in GI K the dip angle was 40°. Experiment GI G was carried out with the 80° plate, but no pre-existing discontinuity was created in the sand. Most of the experiments were repeated at least twice with reproducible results. Table 1 summarizes the key experiments discussed in this contribution and the relevant geometries.

4.1. Materials and scaling

In the experiments, a pure quartz sand of aeolian origin was used (Fontainebleau sand from the Paris Basin, France, angle of internal friction $\varphi \sim 30°$, density $\rho = 1.493$ g cm^{-3}, cohesion $C \sim 500$ Pa; Krantz, 1991). The very low cohesive strength of the sand in dry conditions makes it essentially strain-rate independent, which allows experiments to be performed over reasonable periods of time. In spite of the fact that granular materials obey the Mohr–Coulomb failure criterion, faults that develop in sand are essentially dilatant shear zones (Mandl et al., 1977; Krantz, 1991), where a significant drop in cohesion occurs (of the order of 200–300 Pa). A recent study by Lohrmann et al. (2003) has also shown that the angle of internal friction at peak strength conditions for initially homogeneous materials differs slightly from the angle of friction for already faulted material.

Assuming a thickness of the brittle crust of between 10 and 20 km, a geometric linear scaling factor of 3×10^{-6} was used, so that a 20-km-thick brittle crust scales down to a 60 mm-thick sand pile. Brittle deformation is considered as effectively time independent.

5. Results: strike–slip experiments with a pre-existing discontinuity

5.1. Experiment GI A

In this experiment the pre-existing fault, dipping at an angle of 50°, was located 60 mm from the plate boundary at the base of the model. Fig. 4 shows six stages of the deformation path, starting from the undeformed sand layer to the situation at maximum offset (i.e. 50 mm, equivalent to about 16 km in nature, which equals the maximum sinistral displacement of ~15 km estimated by Viola et al. (2001) for the Giudicarie fault system). GI A0 in Fig. 4 shows the surface expression of the fault discontinuity, artificially created in the model by pulling the stiff metal wire from the base to the surface. Fig. 4 also shows four cross-sections and their position in the deformed model. It is important to note that, given the position of the metallic wire on the plate before the pull, the initial planar discontinuity surface did not cross the imaginary vertical line linking the plate boundary to the surface of the model. The initial planar discontinuity was located above only one of the basal plates.

During early stages of deformation, the first structures to appear were en échelon synthetic Riedel shears, whose surface strike ranged between 30 and 37° with respect to the longitudinal borders. Their right-stepped arrangement was consistent with sinistral shearing. The Riedel shears started to develop in the external part of the model and, with increasing displacement, also nucleated in the middle part. With increasing offset (GI A10–GI A15) new Riedel shears formed and developed at a lower angle than the first generation set (15–17°). At the surface above the plate boundary, displacement was accommodated in the initial stages by bulk shearing of the overburden (see the bending of the red marker lines), followed by rupture and development of a major throughgoing fault zone into which the previously developed Riedel shears converged. A complex pattern of anastomosing shear zones developed, defining isolated lenses and blocks and finally even cutting through major pre-existing structures (first generation Riedels). Many blocks became subdivided by additional secondary ruptures, enabling isolated blocks to move differentially with respect to others. The major displacement was concentrated on the central throughgoing fault, which developed entirely 'north' of the introduced pre-existing fault.

This experiment is only in partial agreement with the results of previous experiments performed to simulate strike–slip regimes. The surface strike angle of the first Riedel shears appearing in the experiment (section GI A10 in Fig. 4) was significantly higher than in similar 'classical Riedel shear experiments' (e.g. Koopman et al., 1987; Richard et al., 1995; Schöpfer and Steyrer, 2001) and in distributed shear experiments (Schreurs, 2003). Although more experiments are needed to understand this phenomenon

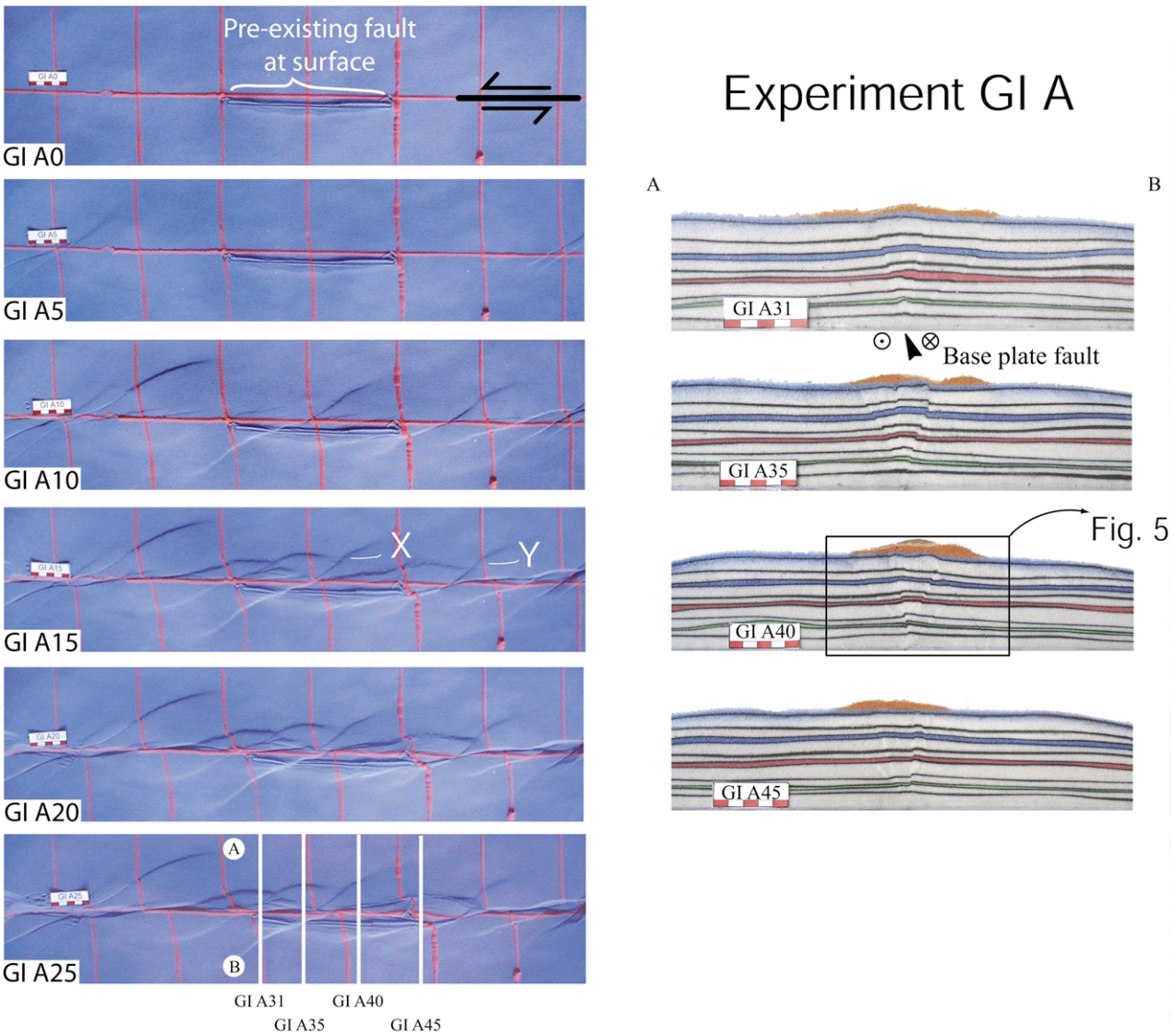

Fig. 4. Photographs showing six stages of deformation for experiment GI A (pure sand, strike–slip experiment, $d = 60$ mm, $\theta = 50°$). The pictures show that the first generation Riedel shear X cuts through the artificial dilation zone without being affected. Riedel Y instead develops exclusively in the 'northern' block and there is no sign of its symmetrical equivalent in the 'southern' block. The strain is partially accommodated by the pre-existing dilation zone. The cross-sections illustrate the development of structures at depth. Scale bar is 50 mm.

better, it seems that the presence of the pre-existing fault hampered the development of early Riedel shears striking on the surface at a lower angle to the imposed strike–slip direction (i.e. the plate boundary). Stress reorientation is likely around the reactivated fault, due to relaxation of shear stresses on the introduced weaker planar zone. In this case, the initial maximum compressive stress may locally be oriented at an angle of more than 45° to the plate boundary, and synthetic Riedel shears will therefore also develop at a higher angle to the boundary.

There are some other interesting features worth noting. In Fig. 4, it is clear that the first generation Riedel shear labelled X cut through the discontinuity on the surface without being affected. The Riedel shear labelled Y, however, developed exclusively in the 'northern' block and there was no sign of its symmetric equivalent in the 'southern' block. Instead, the strain was partially accommodated by the pre-existing fault, as can be seen from the red line, which was sinistrally offset at the tip of the discontinuity. The other red markers cut the pre-existing fault and were offset only by the major throughgoing fault, directly above the plate boundary. There was therefore a partial reactivation of the artificially created fault at the surface. This fact was responsible for the irregular spacing of the Riedel faults in the 'southern' block, which otherwise should be related exclusively to the total thickness of the overburden (Naylor et al., 1986).

Vertical sections cut perpendicular to the base plate fault revealed some other interesting effects due to the pre-existing fault. The expected positive flower structure was well defined by conjugate reverse faults that converged towards the base of the sand, where they were generated. A

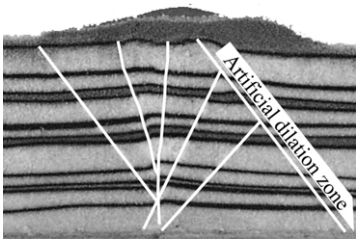

Fig. 5. Enlargement of section GI A40 of Fig. 4.

weak vertical extrusion of the wedge produced a rounded surface bulge. However, the width and opening angle of the flower structure were clearly determined by the old fault structure, which always defined the external boundary of the pop-up in the 'southern' block. In slices GI A35 and GI A40 (Figs. 4 and 5), the artificial cut is clearly recognizable, dipping 50° towards the right. However, whereas in GI A35 it is clear that a steeper reverse fault offset the old fault, in GI A40 it appears that the old fault halted propagation of younger reverse faults (Fig. 5). This apparent contradiction may be explained by considering that, at depth, favourably oriented dip–slip faults are commonly reactivated as strike–slip faults (as already reported by Richard and Krantz (1991)), whereas at the free surface reactivation is less common. In section GI A40, the lack of vertical offset in the layers argues for a predominant strike–slip component. This easier reactivation at deeper structural levels is attributed to a drop in cohesion associated with existing faults, which increases with depth.

5.2. Experiment GI B

This experiment differed from the previous one only in the position of the metallic wire at the base of the sand cake (Table 1). The angle of dip of the pre-existing fault was 52°. As the wire lay closer to the plate boundary (40 mm as against 60 mm in experiment GI A), the surface trace of the introduced discontinuity coincided with the middle red line on the top of the model (Fig. 6). The evolution of the structures in this experiment was similar to that described for GI A. With increasing bulk sinistral shearing, the

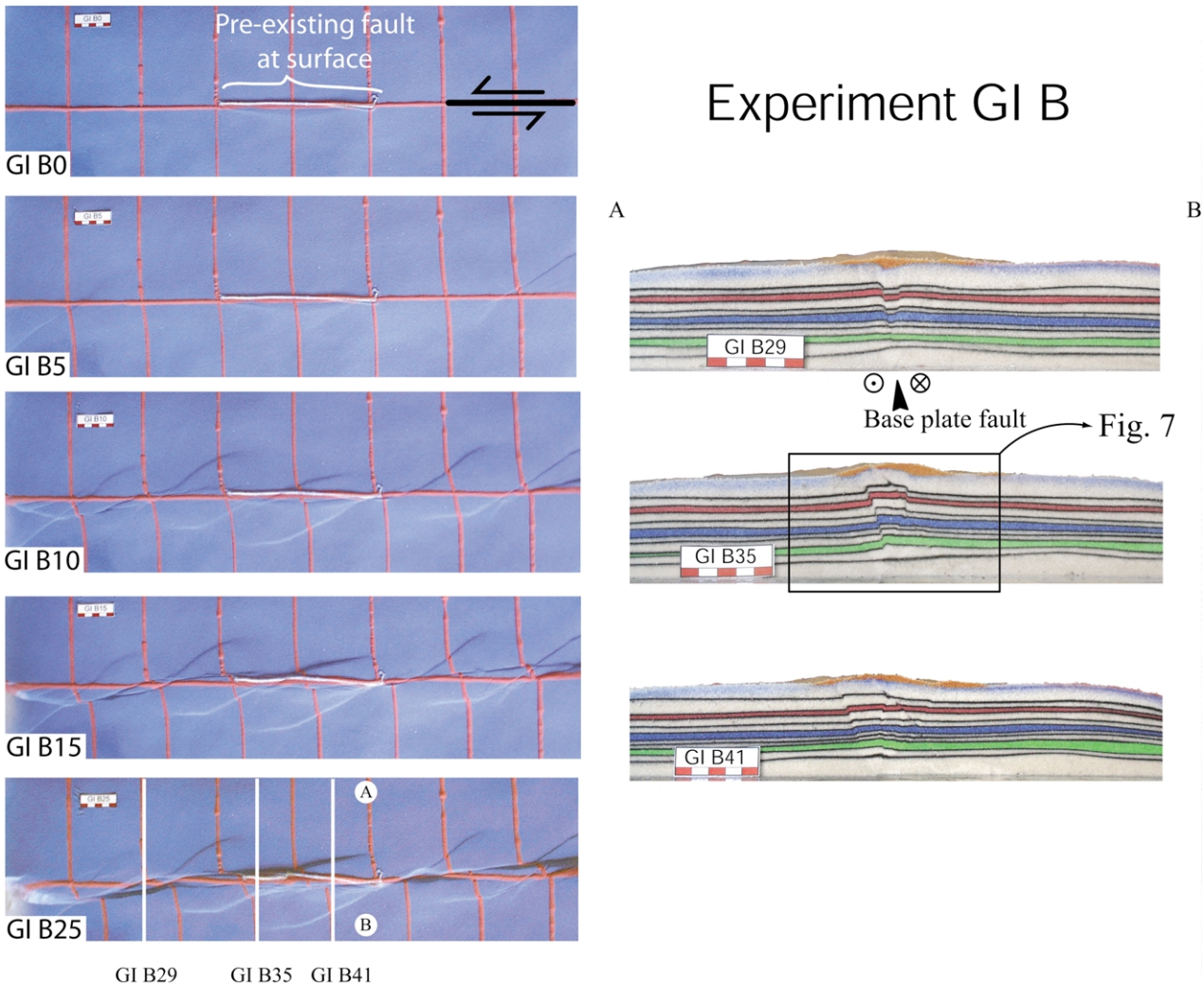

Fig. 6. Plan view and cross-sections of experiment GI B (pure sand, strike–slip experiment, $d = 40$ mm, $\theta = 52°$). Scale bar is 50 mm.

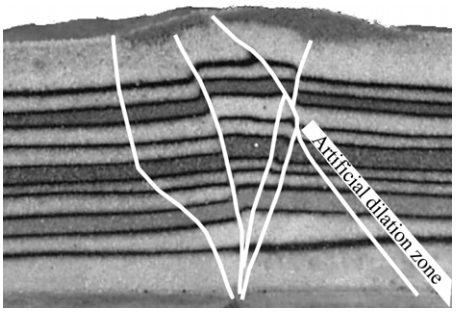

Fig. 7. Enlargement of section GI B35 of Fig. 6.

dominant mechanism of strain accommodation was discrete faulting with synthetic Riedel type structures. These sinistral strike–slip faults had a surface strike between 20 and 38° to the applied shear direction, the highest fault strike being near the unconfined borders. At advanced stages of deformation and progressive shearing (for example GI B15 in Fig. 6), early faults remained active while new faults formed. These newly nucleated shear zones were sinistral strike–slip faults, striking (as observed in GI A) at lower angles than the previously formed Riedel shears, and were arranged in evenly spaced arrays. All structures tended to rotate progressively into the shearing direction, thereby developing a sigmoidal shape in plan view. In the late deformation stages a major throughgoing fault developed, accommodating the largest displacement. Its anastomosing shape defined many isolated units bounded by rotated rupture zones. As can be observed in cross-sections cut perpendicular to the base plate fault (Fig. 6), uplift and subsidence of these small isolated units occurred with apparent irregularity along the strike of the central rupture zone, generating small 'horst and graben' type structures. The deformation appeared to be centro-symmetric, with all the structures evenly distributed on either side of the middle marker line.

The amount of reactivation along the pre-existing discontinuity was not large, as can be deduced from the comparable amount of displacement in the reference grid across the fault trace and in all other sectors of the model along the plate boundary fault. However, section GI B35 in Fig. 6 shows a contribution of the old fault to the total vertical uplift of the sand model in the core of the positive flower structure. A high-angle reverse fault, propagating from the base plate fault, seems to cut the pre-existing discontinuity. A detailed analysis (Fig. 7) showed that the reverse fault actually bends into the old structure and leaves it with an angular discordance with respect to the 'entry' direction. The displacement accommodated by it is also increased in the upper segment, after intersection with the other structure. It is clear that the high-angle reverse fault partially reactivated the older fault, using the already existing low-cohesion plane. The total displacement measured on the surface, visible in the rounded uplifted area, was clearly the sum of the reverse throw components accommodated by both the pre-existing and the newly formed faults.

5.3. Experiment GI C

Fig. 8 presents the spectacular results of experiment GI C, where a complete reactivation of the pre-existing discontinuity was obtained. Fault evolution in this case was markedly different from that in the previous two experiments. In this model the stiff metallic wire was placed immediately above the contact between the two plates (Table 1) and then pulled up to the surface with an angle of 60° to the horizontal, cropping out in the position shown in GI C0 of Fig. 8. Such a location is the best one to achieve fault reactivation because, as described for the previous experiments, all major faults root down into the base plate fault.

Analysis of the experimental results showed that, already at early stages of deformation (for example GI C5 in Fig. 8, corresponding to 10 mm of imposed displacement), the artificial discontinuity exerted a strong influence on the development of structures in the model. A very pronounced asymmetry developed from the onset of deformation, leading to the nucleation of transtensive structures on the left side of the model and transpressive ones in the right part. The intermediate stages of the experiment (GI C15/GI C20 and in the sections in Fig. 8) showed that deformation in the transtensive domain was accommodated by several subvertical normal faults, which propagated in en échelon arrays following the strike direction of the pre-existing discontinuity. The temporal and spatial evolution of these faults produced a series of graben-type structures with a very pronounced subsidence. The creation of space via extension in this sector of the model needed to be compensated by shortening at the opposite tip of the 'old' fault. Indeed, a set of conjugate reverse faults developed, forming a typical positive flower structure (profile GI C47 in Fig. 8). Between these two different structural settings (transtension and transpression) a narrow connection zone developed, largely characterized by pure strike–slip displacement, partially along the old fault (section GI C41 in Fig. 8) and partially along a new vertical fault that propagated very rapidly along the strike direction of the pre-existing fault (section GI C47 in Fig. 8). The key to both uplift and subsidence, which were intermixed within and immediately adjacent to the central zone of movement, was the strike–slip deformation inducing translation of fault-bounded units at various levels. If one unit is driven under another, it causes uplift of the second to produce a welt on the surface whereas, at the same time, it causes subsidence of another unit in its wake, in some cases with associated rotation, as described above. This peculiar behaviour, very different from what was observed in the two previous experiments, was related to the experimental set-up. The initial discontinuity plane dismembered the upper portion of the model in two different sub-blocks that were free to

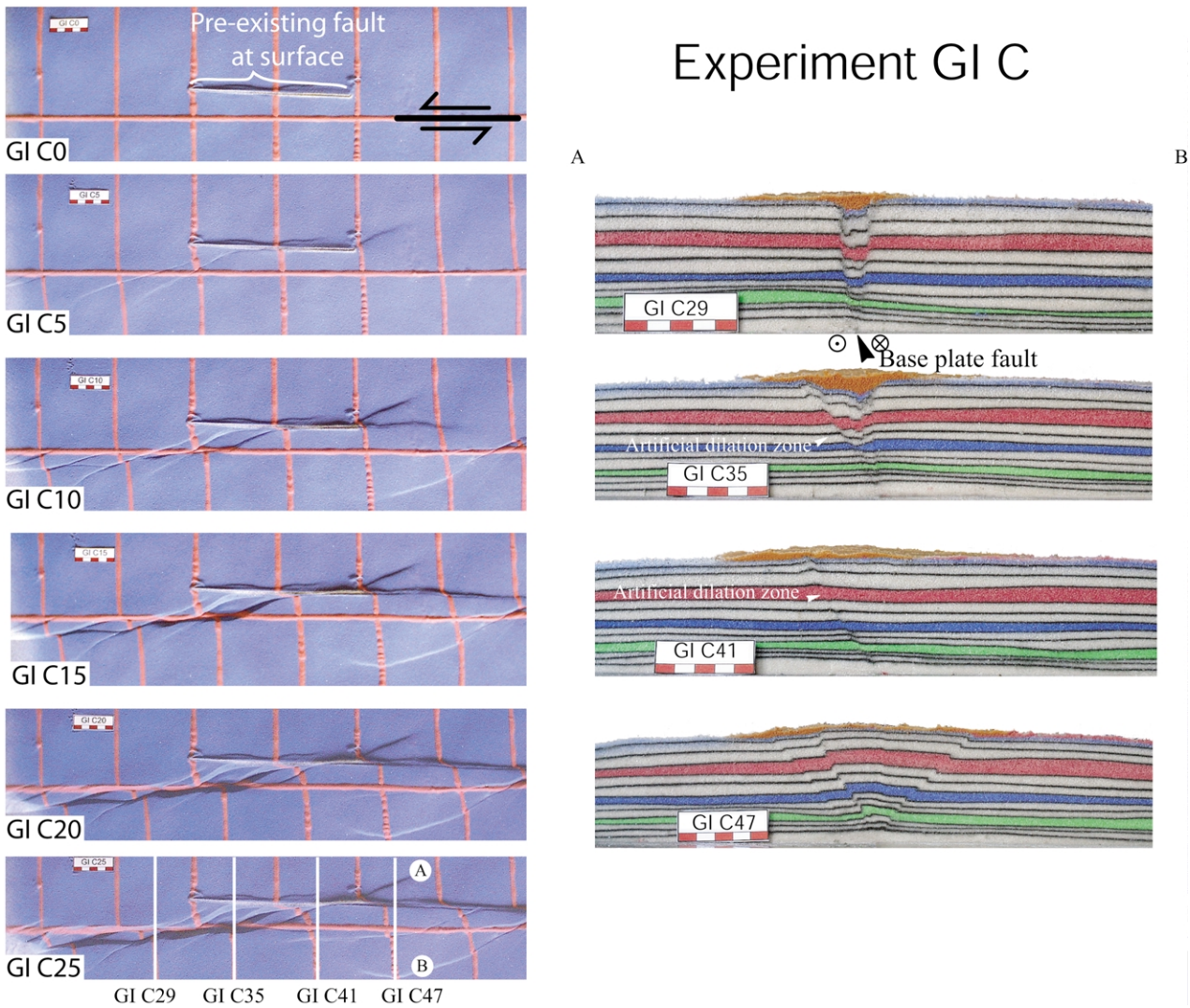

Fig. 8. Plan view and cross-sections of experiment GI C (pure sand, strike–slip experiment, $d = 0$, $\theta = 60°$). Scale bar is 50 mm.

deform independently of each other. On the whole, this experiment showed a deformation pattern, which recalled an 'extrusion' phenomenon towards the right of the small block bounded by the vertical base plate fault and the trace of the pre-existing discontinuity. The latter was actually the dominant structure, controlling the distribution of structures from the early stages of deformation and exerting a dominating influence on the overall geometry.

6. Sinistral transpression experiments

Viola et al. (2001) showed that field evidence points to a transpressional rather than to a pure strike–slip reactivation of the Giudicarie reverse fault in the Late Miocene. Transpression deviates from simple shear by an additional component of shortening perpendicular to the wrench zone. This results in a large variety of three-dimensional structures that can involve complex histories of strain, rotation and associated fabric development. Many theoretical studies have modelled transpression considering either finite or incremental strain (e.g. Sanderson and Marchini, 1984; Fossen and Tikoff, 1993; Tikoff and Teyssier, 1994) or strain rate (Ramberg, 1975). Even for homogeneous models of transpression, such as a perpendicular combination of a pure shear and a simple shear (Sanderson and Marchini, 1984), the resulting deformation path is much more complex than for a simple shear zone. However, these models are idealized compared with the strain patterns in naturally occurring shear zones. Some effort has been made to reproduce more realistic conditions, involving strain gradients (Robin and Cruden, 1994), but the complexity of such theoretical analyses does not allow generalizations to be made concerning finite strain and therefore deformed rocks. One of the most geologically relevant issues in the analysis of transpression regimes is the relationship between the long axis of the strain ellipsoid, i.e. the stretching lineation, and the shearing direction. It is commonly assumed that the finite stretching lineation indicates the direction of tectonic movement in simple shear, at least at high strain. However,

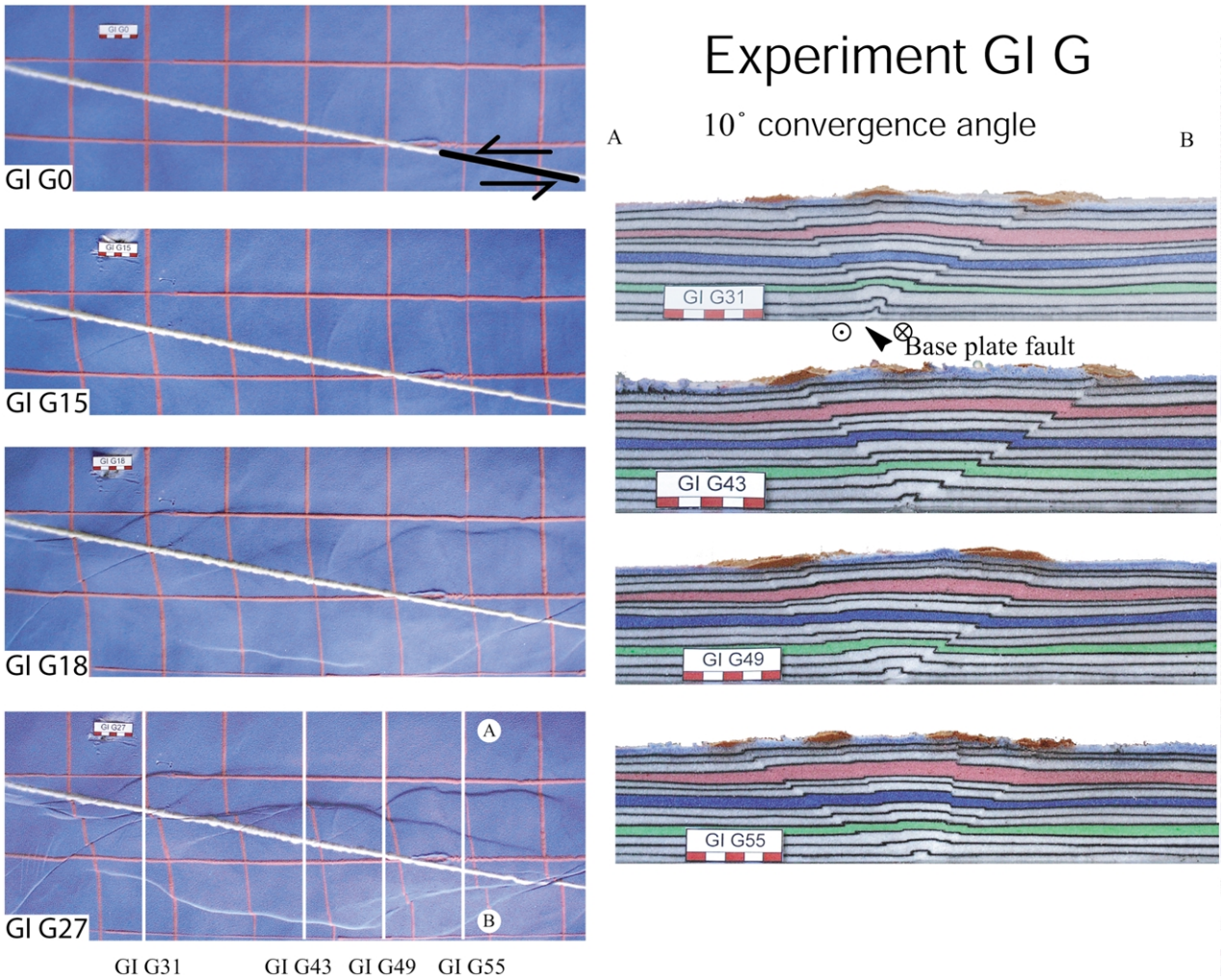

Fig. 9. Photographs in plan view of four deformation stages and four cross-sections of experiment GI G (pure sand, transpression experiment, convergence angle = 10°, no artificial dilation zone). Scale bar is 50 mm.

field studies and theoretical models indicate that stretching lineations can be either horizontal or vertical within transpressional shear zones, according to the angle of convergence between the two colliding blocks. An understanding of transpression is crucial since deformation is often driven by oblique relative motion between lithospheric plates and transpression (and transtension) occur on a wide variety of scales.

In the following experiments, the geometric and kinematic evolution of faulting in zones of transpression is discussed, investigating to what extent the presence of an older discontinuity in the sand model affects the partitioning of strain and fault motions. In order to maximize the reactivation in the transpression experiments, we decided to locate the metal wire on the oblique base plate fault and to investigate this specific set-up.

6.1. Experiment GI G

This experiment was performed with no pre-existing discontinuity, in order to observe the progressive development of faults in a transpressional regime with a convergence angle of 10°. The white line on the model shows the position of the plate boundary projected up to the surface (Fig. 9). As can be seen from Fig. 9, the onset of discrete brittle failure took place only at very advanced stages of deformation. In photograph GI G15 (corresponding to a finite displacement of 26 mm), the model was still being deformed by bulk shearing distributed over a large area, as can be seen from the distortion of the red marker lines. However, once this deformation stage was reached, only a few millimetres of further displacement were needed to cause the development of a pervasive system of faults. These were predominantly thrusts that developed in the 'northern' block, accommodating the shortening component. With increasing deformation they became sinistral, oblique–slip, reverse faults. The uplifted block between the thrust faults (dipping between 35 and 45°) defined a pop-up structure that was roughly parallel to the plate boundary, shown on the surface by the white line. At advanced stages of deformation, a second major thrust developed (GI G27), accommodating the increasing deformation. The interference pattern between the two thrusts defined a second order

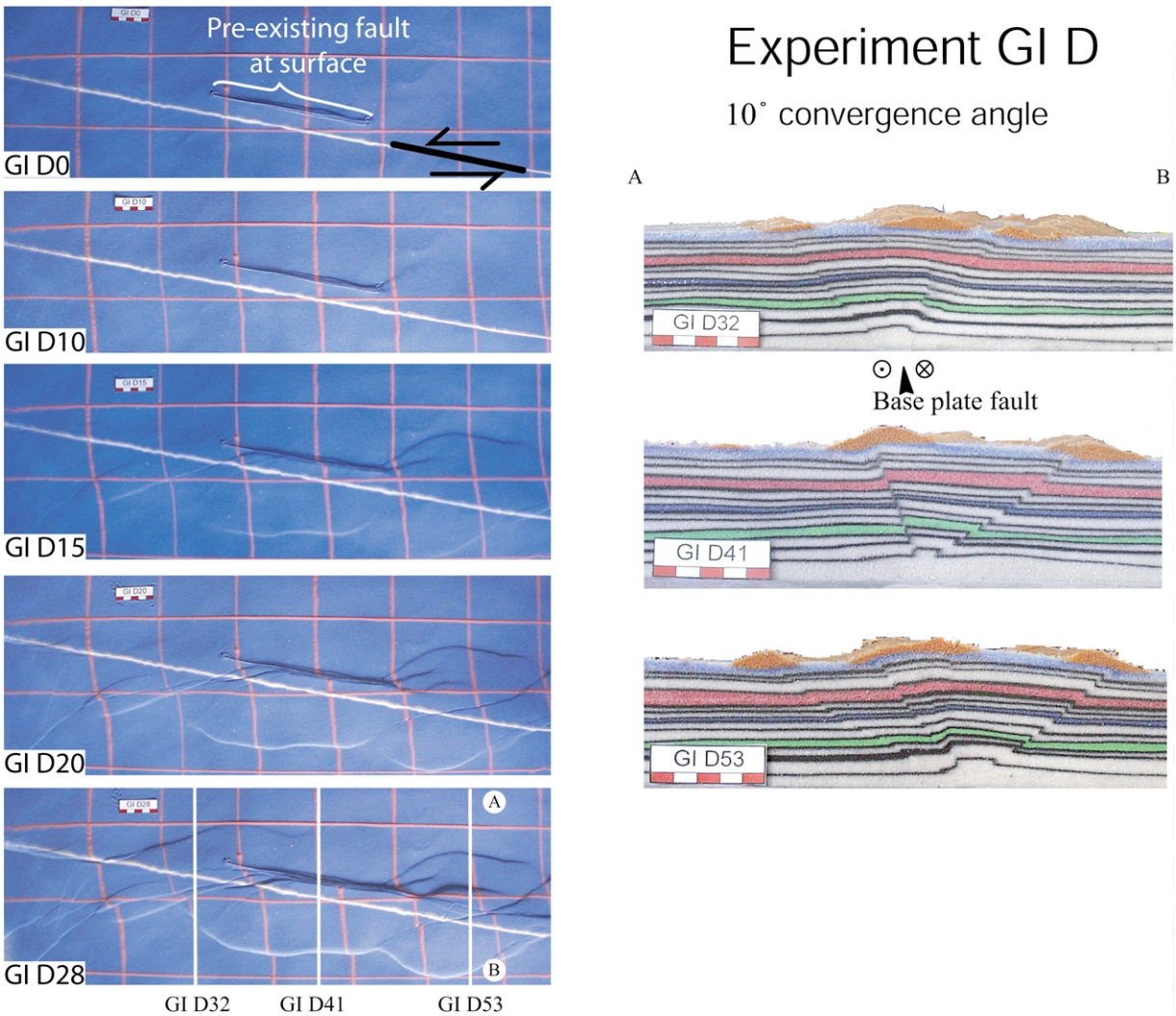

Fig. 10. Photographs of five different deformation stages and cross-section of experiment GI D (pure sand, transpression experiment, convergence angle = 10°, $\theta = 68°$). Note the markedly asymmetric development of the structures. Scale bar is 50 mm.

pop-up (section GI G55 in Fig. 9), which probably reflected partial partitioning of fault displacements at late stages of transpression (GI G27).

The cross-sections showed once again the merging of the faults towards the base plate fault (Fig. 9). Compared with the previous experiments, GI G displayed a prevalence of thrusts that accommodated most of the accumulated shortening and a general lack of Riedel-type faults.

6.2. Experiment GI D

Experiment GI D was performed with a convergence angle of 10° and with an initial discontinuity (dipping 68°) extending from the plate boundary up to the surface (Fig. 10). A very marked reactivation of the old fault was obtained, leading to a very pronounced structural asymmetry between the 'northern' and 'southern' parts of the model, thus confirming the idea that early faults determine, to a large extent, the subsequent fault pattern and fault evolution only if they are favourably oriented for reactivation.

Already at early stages of deformation, a thrust accommodating the shortening component nucleated at the right-hand tip of the slot together with weak but widespread bulk shearing (Fig. 10). With increasing deformation, a series of subvertical sinistral strike–slip faults, which developed in en échelon arrays (Fig. 10), converged near the opposite end of the pre-existing fault. Their displacement was progressively transferred onto the discontinuity, which accommodated both a very large horizontal displacement as well as an important reverse throw (Fig. 10). Section GI D41 (Fig. 10) showed a rather simple structure, where a set of conjugate faults (the artificial dilation zone and a major thrust) formed a positive flower structure. With increasing strain, new thrusts and strike–slip faults developed at the right-hand tip of the pre-existing dilation zone, branching off from the old discontinuity (splay faults). At very late stages of deformation, a subvertical strike–slip

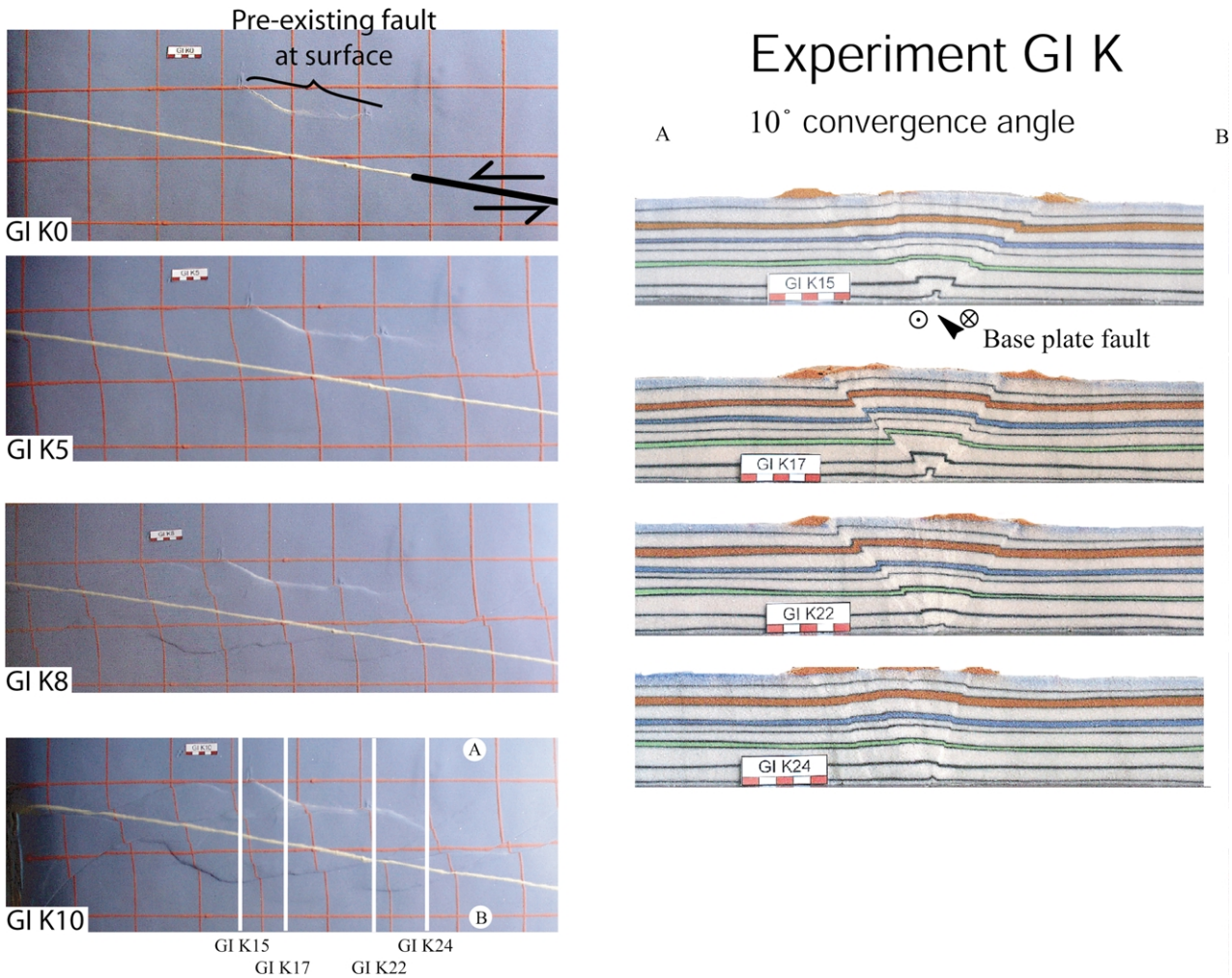

Fig. 11. Plan view and cross-sections of experiment GI K (pure sand, transpression experiment, convergence angle = 10°, $\theta = 36°$). Scale bar is 50 mm.

fault, parallel to the plate boundary, formed from the introduced discontinuity (GI D28 in Fig. 10).

6.3. Experiment GI K

Experiment GI K was performed with the same boundary conditions as GI D. However, in order to reproduce the case of a reactivated, more shallowly-dipping thrust, the metal wire was pulled out from the sand at an angle of 40° to the horizontal. The curved shape of the fault at the surface is again due to the technical difficulty of pulling the wire at a constant angle from the horizontal and is accentuated by the low intersection angle of the introduced discontinuity with the surface.

Until quite advanced stages of deformation (GI K5 in Fig. 11, corresponding to 25 mm displacement), the model was still deformed by bulk shearing distributed over a large area, as can be seen from the distortion of the red marker lines. Again, as in GI G and GI D, only a few millimetres of further displacement resulted in the development of a pervasive system of faults (GI K8). The fault distribution was highly asymmetric, as in the case of experiment GI D. A series of straight, narrow, subvertical strike–slip faults converged asymptotically into the pre-existing fault near its left termination and along its entire length (GI K10). The old discontinuity was partially reactivated and accommodates both strike–slip and reverse displacement. At its right termination, however, there was no sign of any steep strike–slip faults branching off, only a single sinistral transpressive fault dipping at about 40° (section GI K22 in Fig. 11) splayed off. This fault was terminated by a straight Riedel shear, which was kinematically and geometrically linked to a major back-thrust bounding the model on the side of the mobile plate.

6.4. Experiment GI E

This experiment was performed with a convergence angle of 5° and the presence of an initial discontinuity dipping 45°. The formation and growth of the faults basically resembled that described for the strike–slip experiments (Fig. 12). From the onset of deformation, major Riedel shear zones formed and cut through the old fault. However, a minor difference from the strike–slip

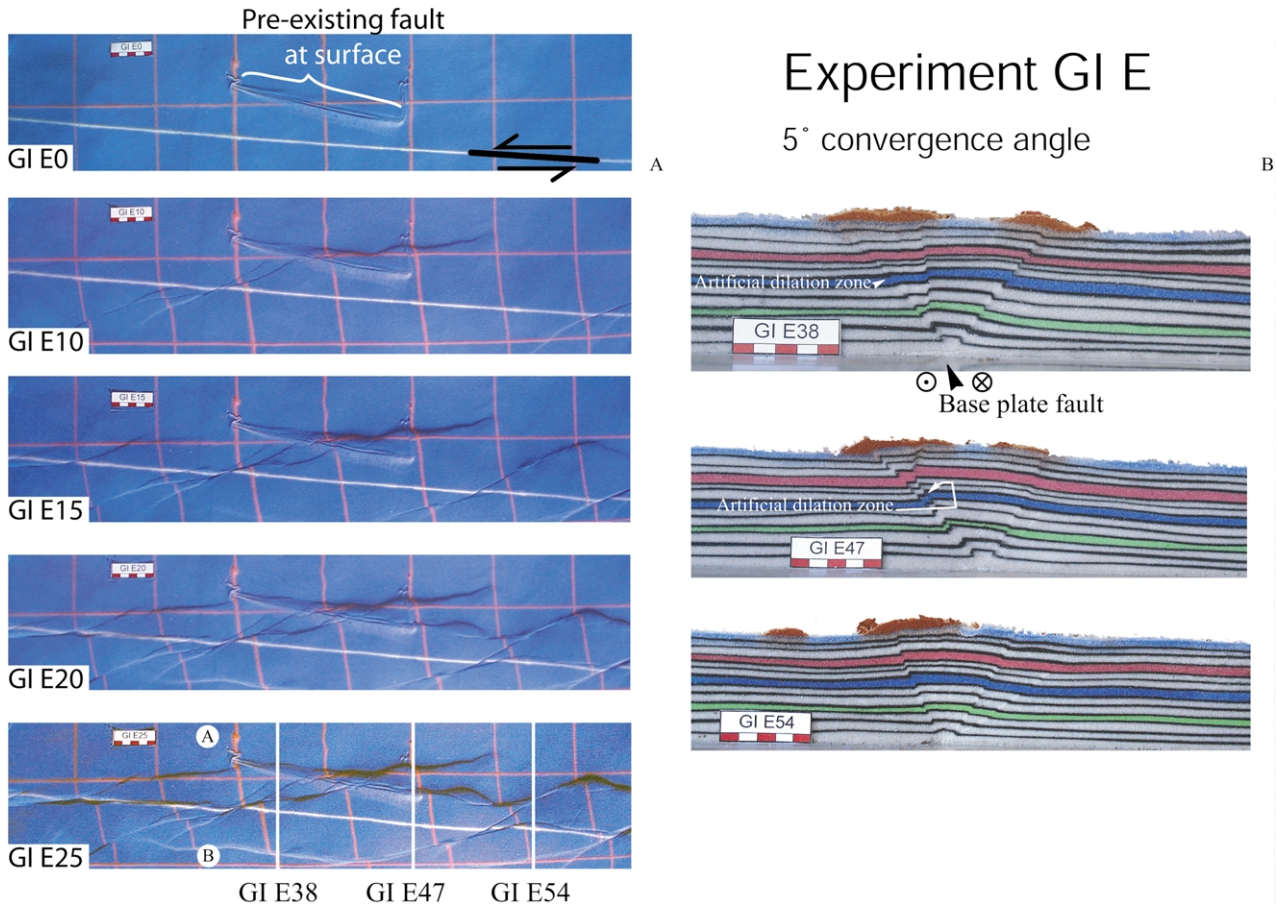

Fig. 12. Plan view and cross-sections of experiment GI E (pure sand, transpression experiment, convergence angle = 5°, $\theta = 45°$). Scale bar is 50 mm. The sudden break in slope of the pre-existing fault close to the surface as visible in section GI E47 is due to the difficulty of extracting the wire from the sand.

experiments was the larger amount of vertical displacement accommodated by the Riedels in the central part of the model. Fig. 12 shows three vertical sections. In GI E47 it is clear that the Riedel faults had a major reverse component and that their sinistral strike–slip offset was rather limited. This reflects the shortening component introduced by the 5° convergence angle. The development during late stages of deformation of the typical backthrust structure was also an expression of the shortening component present in the model.

Fig. 12 shows that, in this model, only a weak reactivation of the pre-existing discontinuity was achieved. The initial fault mainly helped to localize the faults developing at late stages of the deformation. The final deformation phase (GI E25) presented a throughgoing anastomosing fault that did not follow the plate boundary direction (the white surface line). Instead, it was aligned along the strike direction of the pre-existing fault, arguing for a mechanical influence of the old fault during the deformation (compare also with experiment GI G). In section GI E47 (Fig. 12), the pop-up structure was bounded by the backthrust and by a Riedel shear fault, whereas the pre-existing thrust remained bounded within the positive flower structure, in contrast to the other experiments.

7. Discussion and application to the Giudicarie fault system

The degree of reactivation of a pre-existing reverse fault has been shown to be strongly dependent on the position at depth of the reverse fault itself relative to the location of the younger strike–slip fault. The strongest reactivation in the pure strike–slip experiments was achieved in those experiments where the old reverse fault continued upwards from a point immediately above the base plate fault that generated the strike–slip deformation (see experiment GI C). Strong reactivation occurred in this case because the faults rooted into the base plate boundary, implying that they were initiated at depth and progressively propagated upward. The basal drag exerted on the sand by the plates was the probable reason. The sand was completely attached to the base plates and therefore the plate motion produced shear stresses at depth. Hence, the orientation of the principal stress axes needed not necessarily to be vertical or horizontal and faults could be of the oblique–slip type. On the other hand, there were no shear stresses on the free upper surface and therefore two principal stresses were horizontal and the third was vertical (e.g. Anderson, 1951). Failure of a homogeneous brittle material at the surface

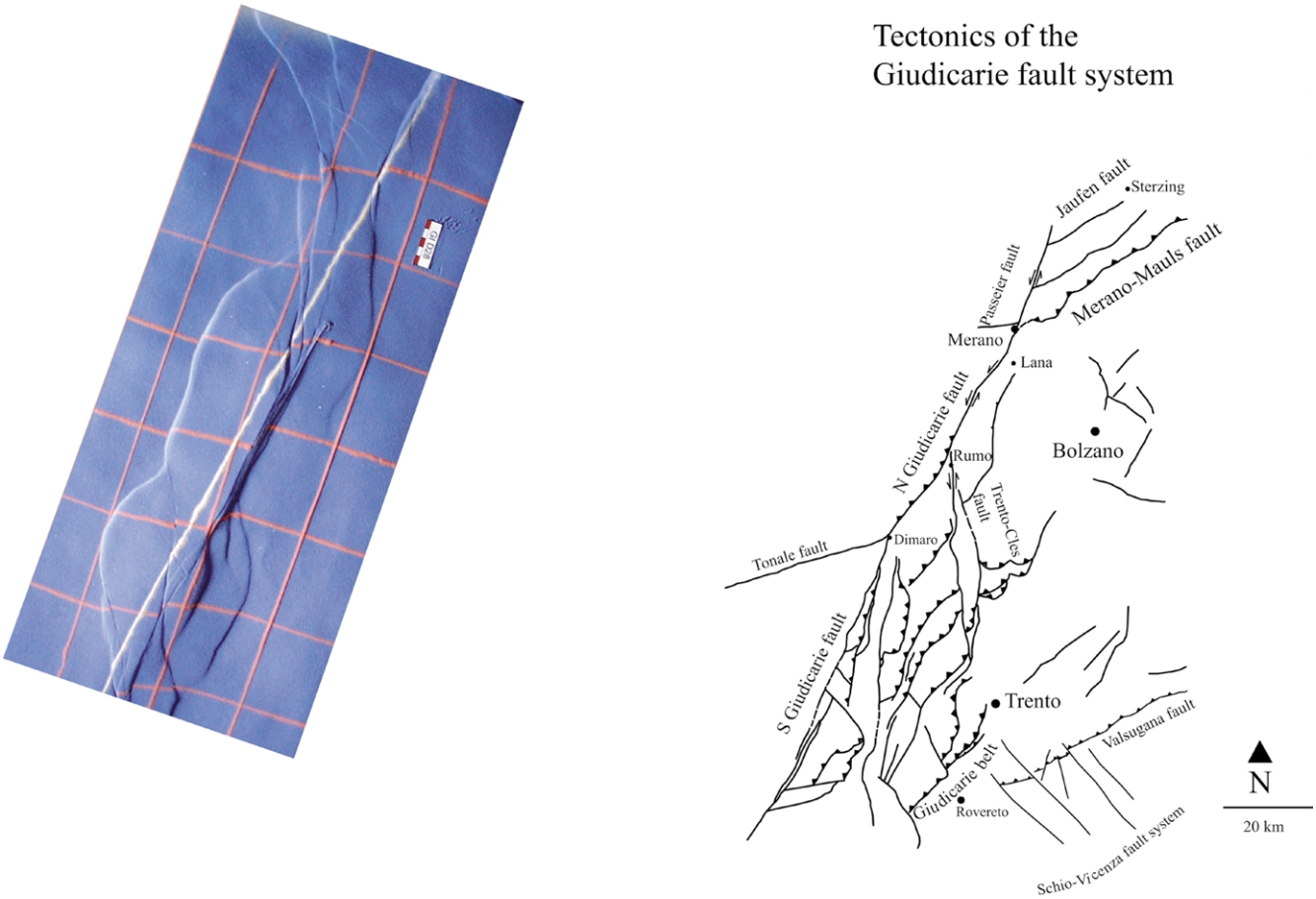

Fig. 13. Comparison between the tectonic map of the Giudicarie fault system and the results of experiment GI D. The experiment was performed in a sinistral transpressive regime with a 10° convergence angle and a pre-existing dilation zone dipping at 68° (cf. Fig. 10). This is the experiment that best reproduced the structures observed in the field.

should therefore produce reverse, normal or strike–slip faults, but not oblique–slip faults. In fact, the faults cropping out on the surface of the models were locally oblique slip faults, which is not in accord with the Andersonian theory. Our experiments used sand throughout the model, without any viscous material capable of decoupling the sand from the drag effect produced by the basal plates. Thus, the imposed stress field at the base of the models had a significant shear stress component parallel to the basal plate, explaining why oblique slip faults occurred at depth from the earliest stages of deformation. Our experiments showed clearly that oblique slip was maintained and accommodated along the entire fault plane, from the base to the upper free surface, satisfying strain compatibility requirements. As discussed by Richard and Cobbold (1990), at the upper free surface of a model where the vertical stress is zero, a cohesionless material can only satisfy Coulomb's criterion if the horizontal stresses are also zero. In this case, the direction of the principal stress axes is undefined and hence faults of any orientation are possible at the free surface. However, this is true only if the deformed granular material is strictly cohesionless (i.e. the failure envelope passes through the origin). In real materials, which will have a finite, even if very small, cohesion (e.g. the sand used here), this argument is not appropriate and the Andersonian theory of failure should still apply. More important in the current application is that this theory only determines the orientation of planes of initial brittle failure. In the models presented here, failure clearly initiated at depth where shear stresses were imposed by the coupled base plate. Oblique–slip faults then propagated upward and kinematic compatibility required that they maintain an oblique–slip component up to the surface.

Schreurs and Colletta (1998), by using a thin layer of PDMS (polydimethylsiloxane, a viscous material with a density of 0.965 g cm^{-3} and a Newtonian viscosity of 5×10^4 Pa s), efficiently decoupled the sand from the basal shear stresses, accommodating initial oblique deformation through either nearly pure strike–slip or nearly pure dip–slip faults. They successfully demonstrated the validity of Anderson's theory, at least for initial faulting, when the base of the model is decoupled.

The reconstruction of the Neogene tectonic activity of the Giudicarie fault system (Viola et al., 2001) showed a twofold deformation history. An early thrusting episode was accommodated along the northern sector of the Giudicarie

fault. This was followed by a period of sinistral transpression, which offset and partially dismembered the previously created thrust structures. The geometry and kinematics of this reactivation were most closely reproduced by experiments GI D and GI K, which involved a mobile plate with a convergence angle of 10° (modelling transpression conditions) and the presence of a pre-existing thrust-type discontinuity in the sand model dipping at 68° for GI D and 40° for GI K, respectively. Field data (e.g. Prosser, 1998; Viola et al., 2001) suggest that the Giudicarie thrust fault plane dips at about 45–55° to the NW, which is intermediate to the dip angles adopted for experiments GI D and GI K.

Fig. 13 compares the tectonic map of the investigated area with the final deformation stage of experiment GI D (see also Fig. 2). Experiment GI K also closely recalled the Giudicarie tectonic scenario. Its general fault pattern and the style of reactivation were similar to those of experiment GI D and to the tectonic map of Fig. 13. However, due to the shallower dip angle of the pre-existing fault (40° as opposed to 68° in experiment GI D), reactivation of the pre-existing thrust was less dramatic.

In general, however, the results of both models can be successfully compared with several major features of the Giudicarie fault system:

1. Model results and nature show a strong asymmetry in the development of the structures with respect to the strike direction of the pre-existing thrust/reverse fault. In the models, the steep faults in the northwestern sector converged into the older weakness zone and were mostly characterized by strike–slip displacements. In nature, this is well represented by the Passeier fault, a NNE–SSW-trending brittle fault with a sinistral transpressive displacement, which in part reactivated the Giudicarie fault (Figs. 2 and 13; Viola et al., 2001). The stretching lineation associated with the Passeier fault shearing is subhorizontal (consistent with the theory; Fossen and Tikoff, 1993); such a geometry argues for a convergence angle smaller than 20° (indeed 10° in GI D). On the tectonic map (Fig. 13), the Passeier fault is marked as a single lineament. However, a more heterogeneous situation can be observed in the field, with a broad zone intensively overprinted by small brittle faults trending subparallel to the Passeier fault itself and to the northern sector of the northern Giudicarie fault (also see GI K10 in Fig. 11).
2. The faults in the southeastern corner of model GI D were mostly characterized by reverse displacements at the front of the structures, whereas the lateral ramps accommodated strike–slip movements. These faults branched off from near the southern tip of the pre-existing discontinuity, progressively taking up the displacement accommodated along this reactivated earlier structure and partitioning into a broader and more complex system. This closely resembled the structural pattern mapped in the field. A major system of splay faults branches off from the northern Giudicarie fault and develops entirely in the Southalpine domain. They form the so-called Giudicarie Thrust Belt (e.g. Prosser and Selli, 1991; Prosser, 1998). Major sinistral, subvertical strike–slip faults with associated frontal thrusts (transport direction towards 110°) developed within a thin-skinned-type tectonic regime in the sedimentary cover of the Southalpine domain. These faults reactivated Jurassic synsedimentary faults that bounded the transitional zone between the 'Trento platform' to the east and the 'Lombard basin' to the west.
3. The 'old' reverse fault in model GI D was strongly reactivated with a major oblique–slip component. Fig. 13 shows the large amount of uplift accommodated by the reverse fault of model GI D. However, the northern tip of the discontinuity was not reactivated, as the newly formed faults converged into the thrust south of it. This portion was therefore not in a suitable position to be mechanically reactivated by the stress field associated with the transpressive deformation. In nature this is the case of the Merano–Mauls fault (Viola et al., 2001), which still preserves the thrust-related structures and does not display any evidence of sinistral strike–slip or transpressive later overprint. A very similar situation was observed in model GI K.
4. Zircon fission-track ages from the basement block west of the Giudicarie fault become progressively older towards the south (from 15 to 28 Ma; Viola et al., 2001). This trend implies a decrease in the total amount of vertical displacement in the fault-bounded block. Model GI D showed that the vertical displacement accommodated by the reverse fault (and responsible for the large exhumation in the northern sector) was transferred and partitioned into a system of three splay faults (Fig. 13). Hence the rocks on the western side of the master fault were progressively exhumed by a smaller and smaller amount, leading to the progressively older ages recorded by the fission-track dating.

A remarkable difference between the natural example and the analogue models is the backthrust, present in the left (western) sector of the sand models and absent in the field area (Fig. 13). As discussed in the previous section, the basal drag (possibly even slightly different on the two halves of the experimental set-up) was the reason for the convergence of the major faults into the base plate fault. However, many analogue sand experiments simulating the push of a rigid indenter into a sand pack have shown that the formation of backthrusts is inhibited by the backstop represented by the thick indenter. Deformation tends to be mostly accommodated by a series of forekinks, whereas backshears are poorly developed and rare (Malavieille, 1984; Calassou et al., 1993; Bonini et al., 1999). There is no field evidence for such a major backthrust in the Giudicarie region. The most probable explanation is that the

rheological difference between the two blocks involved in the transpressive event may have played a 'backstop' role. Given its lithological composition (massive gneisses and amphibolites), the Austroalpine basement (corresponding to the western block in the sand model) is mechanically more competent than the adjacent sedimentary cover of the Southern Alps (the eastern block). During the shortening event, the Austroalpine is likely to have acted as a rigid block, creating a solid obstacle to the nucleation and propagation of thrusts towards the internal part of the system. However, Fellin et al. (2002) recently described the existence of a series of narrow NNE- to NE-trending brittle faults (roughly parallel to the northern Giudicarie fault), which accommodated a NW–SE contractional phase with a top-to-NW kinematics. In the light of our results, these faults can be tentatively linked to the backthrusting phase shown in the models.

8. Conclusions

The reactivation process of thrust/reverse faults under brittle conditions in strike–slip and transpressive regimes, reflecting a change in the regional stress field, has been studied in a series of sandbox experiments. The experimental results confirmed the idea that early faults determine to a large extent the subsequent fault pattern and fault evolution. However, the degree and mode of the reactivation are strongly controlled by the location of the old fault and by its orientation relative to the new stress field. The most spectacular reactivation was achieved in experiments where the position of the pre-existing reverse fault (created by pulling a stiff metal wire through the sand layer) coincided with the position of the new strike–slip or transpressive fault. The experiments have also confirmed that an inherited fault can be successfully modelled by a pre-cut dilatant surface. Along such surfaces there is a reduction in the cohesion and also a possible change in the angle of internal friction, which represents a good analogue of the decrease in shear strength that occurs in nature along planar discontinuities and fractures, facilitating the onset of frictional sliding.

The results of these experiments support the tectonic model proposed by Viola et al. (2001) for the Late Oligocene–Neogene evolution of the Giudicarie fault system in the Italian Eastern Alps. Experiments involving reactivation in a sinistral transpressive mode (convergence angle of 10°) of a pre-existing reverse (GI D) or thrust (GI K) fault, reproduced a deformation pattern that was most comparable with the observed natural structures and exhumation pattern determined from zircon fission-track analysis. A strong reactivation of the pre-existing reverse/thrust fault was obtained, leading to a very pronounced structural asymmetry between the left and the right parts of the model that closely resembled the system of sinistral subvertical splay faults branching off from the Giudicarie fault into the Southern Alps (Fig. 13). It is difficult to explain the present-day structural set-up in the Giudicarie region without a two-stage history of fault reactivation, involving initial reverse/thrust faulting followed by sinistral transpression.

Acknowledgements

The authors are indebted to Christine Chevrier for her valuable help and technical suggestions. Giulio Viola was supported during his stay in France by the ETH research grant no. 0-20-211-96 and ETH is gratefully acknowledged. We thank G. Schreurs and C. Gomes for improving the manuscript with very valuable comments and suggestions.

References

Anderson, E.M., 1951. The Dynamics of Faulting and Dyke Formation with Applications to Britain, Oliver and Boyd, Edinburgh, 191pp.

Betz, D., Durst, H., Gundlach, T., 1987. Deep structural seismic reflection investigations across the northeastern Stavelot–Venn Massif. Annales de la Societe Geologique de Belgique 111, 217–228.

Bigi, G., Cosentino, D., Parotto M., Sartori, R., Scandone P., 1990. Structural model of Italy and gravity map (1:500,000). Quaderni di Ricerche Scientifiche 114, 9 sheets.

Bonini, M., Sokoutis, D., Talbot, C.J., Boccaletti, M., Milnes, A.G., 1999. Indenter growth in analogue models of Alpine-type deformation. Tectonics 18, 119–128.

Calassou, S., Larroque, C., Malavieille, J., 1993. Transfer zones of deformation in thrust wedges: an experimental study. Tectonophysics 221, 325–344.

Castellarin, A., Vai, G.B., 1982. Introduzione alla geologia del Sudalpino. In: Castellarin, A., Vai, G.B. (Eds.), Guida alla Geologia del Sudalpino Centro–Orientale. Guide Geologiche Regionali, Societá Geologica Italiana, Roma, pp. 1–23.

Fellin, G., Martin, S., Massironi, M., 2002. Polyphase Tertiary fault kinematics and Quaternary reactivation in the central-eastern Alps (western Trentino). Journal of Geodynamics 34, 31–46.

Fossen, H., Tikoff, B., 1993. The deformation matrix for simultaneous simple shearing, pure shearing and volume change, and its application to transpression–transtension tectonics. Journal of Structural Geology 15, 413–422.

Frisch, W., Kuhlemann, J., Dunkl, I., Brügel, A., 1998. Palinspastic reconstruction and topographic evolution of the Eastern Alps during late Tertiary tectonic extrusion. Tectonophysics 297, 1–15.

Harding, T.P., 1985. Seismic characteristics and identification of negative flower structures, positive flower structures and positive structural inversion. American Association Petroleum Geology Bulletin 69, 582–600.

Holdsworth, R.E., Strachan, R.A., Magloughlin, J.F., Knipe, R.J. (Eds.), 2001. The Nature and Tectonic Significance of Fault Zone Weakening. Geological Society Special Publication, 186.

Koopman, A., Speksnijder, A., Horsfield, W.T., 1987. Sandbox model studies of inversion tectonics. Tectonophysics 137, 379–388.

Krantz, W., 1991. Measurements of friction coefficients and cohesion for faulting and fault reactivation in laboratory models using sand and sand mixtures. Tectonophysics 188, 203–207.

Laubscher, H.P., 1996. Shallow and deep rotations in the Miocene Alps. Tectonics 15, 1022–1035.

Lohrmann, J., Kukowski, N., Adam, J., Oncken, O., 2003. The impact of analogue material properties on the geometry, kinematics and dynamics

of convergent sand wedges. Journal of Structural Geology 25, 1691–1711.

Malavieille, J., 1984. Modelisation experimentale des chevauchements imbriques: application aux chaines de montagnes. Bulletin de la Societe Geologique de France 26, 129–138.

Mandl, G., de Jong, L.N.J., Maltha, A., 1977. Shear zones in granular material: an experimental study of their structure and mechanical genesis. Rock Mechanics. Supplementum—Felsmechanik 9, 95–144.

McClay, K.R., 1989. Analogue models of inversion tectonics. Geological Society Special Publication 44, 41–59.

Müller, W., 1998. Isotopic dating of deformation using microsampling techniques: the evolution of the Periadriatic fault system (Alps). Ph.D. thesis, ETH, Zürich.

Müller, W., Prosser, G., Mancktelow, N., Villa, I.M., Kelley, P.S., Viola, G., Oberli, F., 2001. Geochronological constraints on the evolution of the Periadriatic Fault System (Alps). International Journal of Earth Sciences 90 (3), 623–653.

Naylor, M.A., Mandl, G., Sijpesteijn, C.H.K., 1986. Fault geometries in basement-induced wrench faulting under different initial stress states. Journal of Structural Geology 8, 737–752.

Prosser, G., 1990. Analisi strutturale e cinematica lungo la linea delle Giudicarie nord tra la Val di Sole e la Val di Non (Trentino occidentale). Studi Trentini di Scienze Naturali: Acta Geologica 67, 87–115.

Prosser, G., 1998. Strike–slip movements and thrusting along a transpressive fault zone: the North Giudicarie line (Insubric line, northern Italy). Tectonics 17, 921–937.

Prosser, G., 2000. The development of the North Giudicarie fault zone (Insubric Line, northern Italy). Journal of Geodynamics 30, 229–250.

Prosser, G., Selli, L., 1991. Thrusts of the Mezzocorona–Mendola Pass area (Southern Alps, Italy); structural analysis and kinematic reconstruction. Bollettino della Società Geologica Italiana 110, 805–821.

Ramberg, H., 1975. Particle paths, displacement and progressive strain applicable to rocks. Tectonophysics 28, 1–37.

Richard, P., Cobbold, P., 1990. Experimental insights into partitioning fault motions in continental convergent wrench zones. Annales Tectonicae 4, 35–44.

Richard, P., Krantz, W., 1991. Experiments on fault reactivation in strike–slip mode. Tectonophysics 188, 117–131.

Richard, P., Naylor, M.A., Koopman, A., 1995. Experimental models of strike–slip tectonics. Petroleum Geoscience 1, 71–80.

Robin, Y., Cruden, R., 1994. Strain and vorticity patterns in ideally ductile transpression zones. Journal of Structural Geology 16, 447–466.

Sanderson, J., Marchini, W.R.D., 1984. Transpression. Journal of Structural Geology 6, 449–458.

Schmid, S.M., Kissling, E., 2000. The arc of the Western Alps in the light of geophysical data on deep crustal structure. Tectonics 19, 62–85.

Schmid, S.M., Pfiffner, O.A., Froitzheim, N., Schönborn, G., Kissling, E., 1996. Geophysical-geological transect and tectonic evolution of the Swiss-Italian Alps. Tectonics 15, 1036–1064.

Schönborn, G., 1992. Alpine tectonics and kinematic model of the central Southern Alps. Memorie di Scienze Geologiche 44, 229–393.

Schöpfer, M.P.J., Steyrer, H.P., 2001. Experimental modelling of strike–slip faulting and the self-similar behavior. In: Koyi, H.A., Mancktelow, N.S. (Eds.), Tectonic Modeling: A Volume in Honour of Hans Ramberg. Geological Society of America Memoir, 193, pp. 21–27.

Schreurs, G., 2003. Fault development and interaction in distributed strike–slip shear zones: an experimental approach. In: Storti, F., Holdsworth, R.E., Salvini, F. (Eds.), Intraplate Strike–Slip Deformation Belts. Geological Society Special Publication, 210, pp. 35–52.

Schreurs, G., Colletta, B., 1998. Analogue modelling of faulting in zones of continental transpression and transtension. Geological Society Special Publication 135, 59–79.

Spiess, R., Marini, M., Frank, W., Marcolongo, B., Cavazzini, G., 2001. The kinematics of the Southern Passeier fault: radiometric and petrographic constraints. Schweizerische Mineralogische und Petrographische Mitteilungen 81, 197–212.

Tikoff, B., Teyssier, C., 1994. Strain modeling of displacement-field partitioning in transpression orogens. Journal of Structural Geology 16, 1575–1588.

Viola, G., Mancktelow, N.S., Seward, D., 2001. Late Oligocene-Neogene evolution of Europe-Adria collision: new structural and geochronological evidence from the Giudicarie fault system (Italian eastern Alps). Tectonics 20, 999–1020.